Direct numerical simulations of mass transfer in square microchannels for liquid-liquid slug flow

Nathalie Di Miceli Raimondi [a], Laurent Prat [a,b,*], Christophe Gourdon [a,b], Patrick Cognet [a,b]

[a] Chemical Engineering Laboratory of Toulouse UMR 5503 CNRS/INP/UPS, 5 rue Paulin Talabot, 31106 Toulouse Cedex 01, France
[b] University of Toulouse, INP-ENSIACET, France

Abstract

Microreactors for the development of liquid-liquid processes are promising technologies since they are supposed to offer an enhancement of mass transfer compared to conventional devices due to the increase of the surface/volume ratio. But impact of the laminar flow should be negative and the effect is still to be evaluated. The present work focuses on the study of mass transfer in microchannels by means of 2D direct numerical simulations. We investigated liquid-liquid slug flow systems in square channel of 50 to 960 µm depth. The droplets velocity ranges from 0.0015 to 0.25 m/s and the ratio between the channel depth and the droplets length varies between 0.4 and 11.2. Droplet side volumetric mass transfer coefficients were identified from concentration field computations and the evolution of these coefficients as a function of the flow parameters and the channel size is discussed. This study reveals that mass transfer is strongly influenced by the flow structure inside the droplet. Moreover, it shows that the confinement of the droplets due to the channel size leads to an enhancement of mass transfer compared to cases where the droplets are not constrained by the walls.

Keywords: microchannel; multiphase flow; mass transfer; computation; mathematical modelling

1. Introduction

Within the frame of processes intensification, the use of micro-technologies to carry out two-phase operations has been intensively studied since they can strongly enhance mass transfer compared to conventional devices (Stankiewicz and Moulijn, 2000; Jänisch et al., 2004). This enhancement is mainly due to their ability to produce high interfacial area. Indeed, Yue et al. (2007) reviewed the specific interfacial area produced by different gas-liquid contactors: in conventional devices, it can reach up to around 2000 m^2/m^3, while Hessel et al. (2005) have generated interfacial area up to 20000 m^2/m^3 with gas-liquid slug flows in microstructured monoliths. In addition, as a result of the microchannels size, diffusion times are very short which minimizes the mass transport limitations to the benefit of chemistry.
For the development of microreactors to carry out liquid-liquid processes, mass transfer coefficients must be consistently estimated to obtain a reliable process design. Few works focused on liquid-liquid mass transfer using slug flow in microchannels: Burns and Ramshaw

* Corresponding author. Tel.: +33 5 34 61 52 59; fax: +33 5 34 61 52 53
E-mail address: Laurent.Prat@ensiacet.fr

(2001) studied the titration of acid acetic which was controlled by the acid transfer from kerosene to a basic aqueous solution. This reaction was carried out in a square microchannel of 380 μm depth using slug flow. They obtained an increase of the global mass transfer coefficient with the flow velocity. Dummann et al. (2003) observed the same tendency while carrying out the nitration of single ring aromatics in circular capillaries of 0.5 and 1.0 mm diameter. However, no model was suggested to estimate mass transfer coefficients in such systems. Nevertheless, two cases have been intensively studied as described afterwards: (1) liquid-liquid mass transfer in macrochannels and (2) gas-liquid mass transfer in microchannels.

For liquid-liquid mass transfer in macrochannels, numerous empirical correlations to predict dispersed phase mass transfer coefficients k_d have been established (Knudsen et al., 1998; Slater, 1994). However, in order to approach microchannel flow conditions, we should focus on circulating droplets, i.e. with internal recirculation loops, with non-oscillating interface (Kashid et al., 2005). An empirical correlation was proposed by Skelland and Wellek (1964):

$$Sh_d = \frac{k_d d_d}{D_d} = 31.4\, Re_d^{\,0.371}\, Ca_d^{\,0.371} Fo_d^{\,-0.338} Sc_d^{\,-0.125} \quad (1)$$

where d_d is the diameter of a sphere with the same volume than the droplets, D_d the molecular diffusion coefficient of the solute in the dispersed phase. The dimensionless numbers are particle numbers, calculated with a characteristic length equals to d_d.

In the case of gas-liquid system in microchannels, we can distinguish two types of models: the first one based on empirical correlations, and the second one based on theory. Both of them allow the estimation of continuous phase mass transfer coefficients since the resistance to the transfer in the gas phase is negligible compared to the one in the liquid phase. Berčič and Pintar (1997) proposed to estimate liquid volumetric mass transfer coefficient k_La using the following correlation:

$$k_L a = \frac{0.111 \cdot U_d^{\,1.19}}{\left((1-\varepsilon_G)\cdot L_{UC}\right)^{0.57}} \quad (2)$$

where U_d represents the bubble velocity, ε_G the gas hold-up, and L_{UC} the unit cell length (Figure 1). They deduced this correlation from experimental results obtained in circular capillaries of 1.5 to 3.1 mm diameter. As it can be seen in Eq.2, it does not consider the influence of the channel diameter w_C on the mass transfer coefficient.

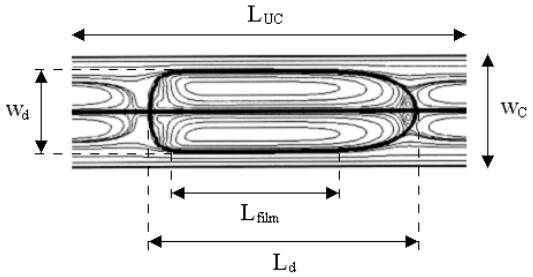

Fig. 1. Illustration of a unit cell for slug flow in a microchannel (Sarrazin et al., 2006).

Irandoust et al. (1992), Kreutzer (2003) and van Baten and Krishna (2004) used a more fundamental approach to estimate k_La in monolith reactors with circular channels. They consider that gas-liquid mass transfer in those devices was the result of two contributions:

from the gas phase to the liquid film surrounding the bubbles $k_{L,film}a_{film}$, and to the liquid slugs through the two bubble caps $k_{L,cap}a_{cap}$:

$$k_L a = k_{L,cap} a_{cap} + k_{L,film} a_{film} \tag{3}$$

$k_{L,cap}$ is then calculated according to Higbie penetration theory, which leads to the following equation in circular channels:

$$k_{L,cap} a_{cap} = \left(2\sqrt{2\frac{D_c U_d}{\pi^2 w_d}} \right) \cdot \left(\frac{\pi \cdot w_d^{\,2}}{L_{UC}\left(\pi \cdot w_C^{\,2}\right)/4} \right) \approx \frac{8\sqrt{2}}{\pi} \sqrt{\frac{D_c U_d}{w_C L_{UC}^{\,2}}} \tag{4}$$

This model assumes that the film is very thin compared to the channel diameter. Therefore, the slug diameter w_d can be approximated by the channel diameter w_C. Van Baten and Krishna (2004) estimated the film contribution by referring to the modelling of mass transfer from a bubble to a laminar falling film. Mass transfer coefficient in this case can be written in terms of Eq.5 or Eq.6 according to Fourier number Fo_{film} given by Eq.7. $t_{e,film}$ stands for the contact time of a fresh liquid element at the film interface (Eq.9).

$$k_{L,film} = 2\sqrt{\frac{D_c}{\pi \cdot t_{e,film}}} \frac{\ln(1/\Delta)}{1-\Delta} \qquad Fo_{film} < 0.1 \text{ (short contact)} \tag{5}$$

$$k_{L,film} = 3.41\frac{D_c}{\delta_{film}} \qquad Fo_{film} > 1 \text{ (long contact)} \tag{6}$$

$$Fo_{film} = \frac{D_c}{t_{e,film} \cdot \delta_{film}^{\,2}} \tag{7}$$

$$\Delta = 0.7857 \cdot \exp(-5.121 \cdot Fo_{film}) + 0.1001 \cdot \exp(-39.21 \cdot Fo_{film}) + ... \tag{8}$$

$$t_{e,film} = \frac{L_{film}}{U_d} \tag{9}$$

Finally, the film interfacial area a_{film} can be written in terms of Eq.10.

$$a_{film} = \frac{\pi \cdot w_d L_{film}}{L_{UC}\left(\pi \cdot w_C^{\,2}\right)/4} \approx \frac{4L_{film}}{w_C L_{UC}} \tag{10}$$

Van Baten and Krishna compared these correlations with gas-liquid mass transfer simulations in circular capillary. They obtained good predictions of k_La over a wide range of parameters values (w_C = 1.5, 2 and 3 mm; L_{UC} = 0.015 to 0.05 m; U_d = 0.15 to 0.55 m/s; ε_G = 0.136 to 0.5). Vandu et al. (2005) fitted experimental results obtained with air and water in circular and square capillaries with van Baten and Krishna model: they showed that the film contribution was the major contribution to mass transfer with their operating conditions (w_C = 1, 2 and 3 mm; L_{UC} = 0.005 to 0.06 m; U_d = 0.09 to 0.65 m/s). Indeed, they neglected the caps contribution and obtained a reasonable agreement between the model and their experiments when $(U_d/L_d)^{0.5} > 3\ s^{-0.5}$ which corresponds to short contact times.

Regarding liquid-liquid systems in microchannels, the hydrodynamic of the dispersed phase seems more complex compared to gas-liquid flows. Sarrazin et al. (2007) showed that the flow structures developed in droplets was strongly influenced by the Reynolds and the capillary numbers (internal velocity profiles, number of recirculation loops). This may lead to

different behaviours in terms of mass transfer. In the present work, two-dimensional (2D) direct numerical simulations allow the study of mass transfer in square microchannels for liquid-liquid slug flow. The influence of various flow parameters and the channel size on the mass transfer coefficient is considered in order to obtain a better understanding and prediction of this transport mechanism at such scale. The reliability of the existing models that are likely to estimate mass transfer coefficients in the system we studied is discussed.

2. Numerical simulations

2.1. General description of the method

The simulations were carried out in two steps: at first, the hydrodynamic behaviour of the system is computed by mean of a research code developed in the Interface group at the Institute of Fluid Mechanics of Toulouse (IMFT - University of Toulouse, France): JADIM (Legendre and Magnaudet, 1998). This numerical tool allows the description of the physical mechanisms present in two-phase flows, resolving continuity and Navier-Stokes equations. In a second step, the concentration field of a solute initially present in the dispersed phase is computed with a code developed and executed with Matlab 7.4.
The numerical method is an interface-capturing technique without any interface reconstruction. The equations and balances are integrated in space using a finite-volume method. The two-phase flow is described using the one-fluid approach where a continuous function φ, so called the volume fraction, allows the phases tracking: it equals zero in the continuous phase and one in the dispersed phase.
Sarrazin et al. (2006) validated the reliability of JADIM code to obtain velocity fields in microchannels in the case of liquid-liquid slug flow. Indeed, a good agreement between simulation results and micro-particle image velocimetry (micro-PIV) measurements is observed. They also demonstrated that the hydrodymamic structure of slug flow in square microchannel could be well estimated using 2D simulations. Indeed, comparing the velocity fields computed with JADIM performing 3D and 2D simulations showed that the flow structures obtained with both kinds of simulations were similar. Consequently, this work exclusively focused on the calculation of hydrodynamic parameters and concentration field over 2D computational domains. The equations are computed over an orthogonal cell-centred mesh refined in the film over the y-axis (near the wall, i.e. y = 0 m), and uniform over the x-axis as illustrated on Figure 2. The length of the computational domain corresponds to a unit cell.

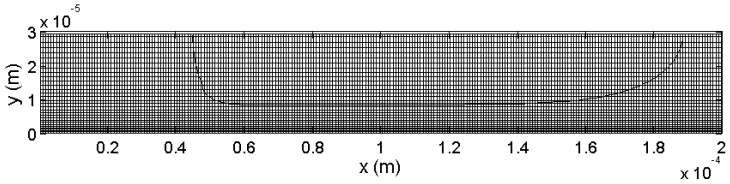

Fig. 2. 2D computational mesh. The thick line represents the fictitious interface obtained with JADIM.

This method assumes that (1) the fluids in both phases are perfectly immiscible, (2) they are Newtonian and incompressible, (3) the physical properties of both phases are constant and not influenced by the solute transfer, (4) the solute transfer does not affect the flow structure: the computations of the system hydrodynamics and the concentration field are decoupled, (5) the gravity effects are negligible at such scale, (6) Marangoni effects are not taken into account, (7) the two-phase flow and the concentration field are planar symmetric (the computational

domain is half a unit cell as shown in Figure 2). The assumptions (3), (4) and (6) are consistent as far as the solute concentration is low.

2.2. Hydrodynamics computation

The hydrodynamics of the system is described using the one-fluid formulation of the continuity and Navier-Stokes equations respectively given by Eq.11 and Eq.12:

$$\nabla \cdot \mathbf{u} = 0 \tag{11}$$

$$\rho\left(\frac{\partial \mathbf{u}}{\partial t} + \mathbf{u} \cdot \nabla \mathbf{u}\right) = -\nabla P + \nabla \cdot \mathbf{T} - \sigma(\nabla \cdot \mathbf{n})\mathbf{n}\delta_I \tag{12}$$

where **u** and P are the local velocity and pressure. **T** stands for the viscous stress tensor. **n** represents the unit vector normal to the interface (directed toward the continuous phase), and δ_I the Dirac-delta-function which equals one at the interface and zero elsewhere. The local density of the system ρ is evaluated using the local volume fraction φ which obeys Eq.13.

$$\frac{\partial \varphi}{\partial t} + \mathbf{u} \cdot \nabla \varphi = 0 \tag{13}$$

$$\rho = \varphi\rho_d + (1-\varphi)\rho_c \tag{14}$$

T is related to the velocity gradient by means of a fourth-order viscosity tensor which depends on a linear viscosity μ_l given by Eq.15 which allows the description of the stresses normal to the interface, and a harmonic one μ_h to insure the shear continuity at the interface (Eq.16). In the case of incompressible fluid and in a 2D representation, the expression of the viscous stress tensor coefficients can be written in terms of Eq.15, where **S** is the strain tensor and n the coefficients of the unit vector normal to the interface **n**.

$$T_{ij} = 2\mu_l S_{ij} + 2(\mu_l - \mu_h)\sum_{p=1}^{2}\sum_{q=1}^{2}\left(S_{ij}n_p n_j + S_{jp}n_p n_i - 2S_{pq}n_p n_q n_i n_j\right) \tag{15}$$

$$S_{ij} = \frac{1}{2}\left(\frac{\partial u_i}{\partial x_j} + \frac{\partial u_j}{\partial x_i}\right) \tag{16}$$

$$\mu_l = \varphi\mu_d + (1-\varphi)\mu_c \tag{15}$$

$$\mu_h = \frac{\mu_d\mu_c}{\varphi\mu_c + (1-\varphi)\mu_d} \tag{16}$$

The capillary force is transformed into a volume force using the continuum surface force model suggested by Brackbill et al. (1992):

$$\sigma(\nabla \cdot \mathbf{n})\mathbf{n}\delta_I = \sigma\nabla \cdot \left(\frac{\nabla\varphi}{\|\nabla\varphi\|}\right)\nabla\varphi \tag{17}$$

The spatial discretisation and time-advancement algorithm used in JADIM code to solve the previous equations is detailed by Bonometti (2005). The spatial discretisation is performed using second-order centred differences. Time advancement is executed using a third-order Runge-Kutta method for the advective and the source terms, and a Crank-Nicholson method

for the viscous terms. The overall algorithm is second-order accurate in time and space. The study of a droplets chain is reduced to the study of a single droplet assuming periodic conditions at the boundaries normal to the flow. The volume of the two phases in the computational domain is initially set. The fluid motion is driven by imposing a pressure gradient between the two boundaries normal to the flow. The computation gives the velocity and pressure fields and the volume fraction. Then, these parameters are used to obtain the concentration field of a solute that transfers from the droplet to the continuous phase.

2.3. Concentration field computation

2.3.1. Mathematical formulation

The concentration field C over the computational domain is governed by the general convective diffusive equations. The transferred flux is expressed using Fick's law leading to the following balances in each phase:

$$\frac{\partial C_d}{\partial t} + \mathbf{u'} \cdot \nabla C_d = D_d \nabla^2 C_d \tag{18}$$

$$\frac{\partial C_c}{\partial t} + \mathbf{u'} \cdot \nabla C_c = D_c \nabla^2 C_c \tag{19}$$

where D is the mass diffusion coefficient. **u'** is the velocity field in a frame of reference moving with the droplets. The subscripts d and c respectively stand for the dispersed and the continuous phases. The concentration at the interface obeys the interfacial equilibrium, m being the distribution coefficient of the solute considered as constant:

$$C_d = mC_c \quad \text{at the interface} \tag{20}$$

To solve these equations according to the one-fluid approach, some transformations must be done to make the concentration at the interface continuous. For that purpose, it is proposed to operate some changes in the concentrations formulation such as:

$$\hat{C}_d = C_d / \sqrt{m} \qquad \hat{C}_c = C_c \sqrt{m} \tag{21}$$

This method is described by Yang and Mao (2005) who simulated interphase mass transfer using the level set approach. Using these transformations, Eq.18, Eq.19 and Eq.20 can be rewritten as follows:

$$\sqrt{m}\frac{\partial \hat{C}_d}{\partial t} + \sqrt{m}\mathbf{u'} \cdot \nabla \hat{C}_d = D_d \sqrt{m} \nabla^2 \hat{C}_d \tag{22}$$

$$\frac{1}{\sqrt{m}}\frac{\partial \hat{C}_c}{\partial t} + \frac{1}{\sqrt{m}}\mathbf{u'} \cdot \nabla \hat{C}_c = \frac{D_c}{\sqrt{m}} \nabla^2 \hat{C}_c \tag{23}$$

$$\hat{C}_d = \hat{C}_c \quad \text{at the interface} \tag{24}$$

Therefore, mass transport in the whole computational domain can be described by only one equation (Eq.25), transforming the parameters t, u and D as shown by Eq.26 to Eq.28. The concentration field is computed through the parameter $\hat{C}$.

$$\frac{\partial \hat{C}}{\partial \hat{t}} + \hat{\mathbf{u}}' \cdot \nabla \hat{C} = \hat{D} \nabla^2 \hat{C} \tag{25}$$

$$\hat{t} = \sqrt{m}\, t + \left(\frac{t}{\sqrt{m}} - \sqrt{m}\, t \right) \varphi \tag{26}$$

$$\hat{\mathbf{u}}' = \frac{\mathbf{u}'}{\sqrt{m}} + \left(\sqrt{m}\, \mathbf{u}' - \frac{\mathbf{u}'}{\sqrt{m}} \right) \varphi \tag{27}$$

$$\hat{D} = \frac{D_c D_d}{\varphi \left(D_c / \sqrt{m} \right) + (1 - \varphi) D_d \sqrt{m}} \tag{28}$$

Initial condition

The solute is initially present in the dispersed phase with a concentration C^0. The continuous phase is pure:

$$\hat{C} = \frac{C^0}{\sqrt{m}} \varphi \quad \text{at } t = 0 \text{ s} \tag{29}$$

Boundary conditions

At the wall and at the symmetry plan, there is no mass flux over the y-direction:

$$\frac{\partial \hat{C}}{\partial y} = 0 \quad \text{for } y = 0 \text{ and } y = w_C / 2 \tag{30}$$

For the boundaries normal to the flow, we introduce two fictitious columns outside the domain which are considered at the same concentration that the boundaries to calculate the convective and the diffusive terms.

2.3.2. Numerical method and procedure

Eq.25 is explicitly integrated over time. The computation algorithm is first-order accurate in time. The diffusive term is second order approximated. The convective term is discretised according to an upwind scheme.

Due to the recirculation loops in the continuous phase between the droplets (see part 3), the solute transferred from one droplet to the continuous phase will impact on the solute transfer from the following droplet. Therefore the slugs can not be considered as single and a set of droplets needs to be simulated. For that purpose, the concentration field over one unit cell is computed according to an algorithm based on an eulerian framework. Considering the flow periodic, with a periodicity T, the algorithm compared the concentration field obtained in a cell at time $t_k = t_0 + kT$ and $t_{k+1} = t_0 + (k+1)T$. The steady state in the cell is supposed to be reached if for each node of the domain the following criterion is satisfied:

$$\frac{\left| C(t_k) - C(t_{k+1}) \right|}{C(t_k)} < 0.01 \quad \text{if } C(t_k) \neq 0 \tag{31}$$

$$\left| C(t_k) - C(t_{k+1}) \right| < 0.01 \quad \text{if } C(t_k) = 0 \tag{32}$$

Once the steady state is reached, the same algorithm is applied to compute the concentration field over the following cell.

2.4. Validation of the numerical method

The methodology previously described has been implemented on different grids. Half a 60 µm depth channel with a computational length of 100 µm is described by a node number of 125×30, 250×30, 125×75, 160×75 and 125×100 (x- direction × y- direction). The influence of the mesh grid size on both hydrodynamics and mass transfer computations is studied. For that purpose, several criteria are evaluated for each simulation case and compared: the droplets and the continuous phase velocities respectively calculated by means of Eq.33 and Eq.34, and the mass transfer coefficient which is directly correlated to the mean droplet concentration profile over time (its estimation from the computed concentration field is described in part 3.1).

$$U_d = \frac{\iint \varphi \cdot (\mathbf{u} \cdot \mathbf{n}) \cdot dxdy}{\iint dxdy} \tag{33}$$

$$U_c = \frac{\iint (1-\varphi) \cdot (\mathbf{u} \cdot \mathbf{n}) \cdot dxdy}{\iint dxdy} \tag{34}$$

Table 1 shows that the mesh grids where the depth of the computational domain is represented by means of only 30 nodes give results that are strongly different that those obtained with finer grids over the y-axis (at least 75 nodes). Indeed, while the computed velocities are not highly dependent on the mesh size (10% increase by doubling the node number over the y-axis), the mass transfer coefficient decreases of more than 30% between the finest and the thickest mesh grids. This difference is mainly due to the truncation error implied by the discretisation of the advective term in Eq.25. This error acts like a diffusive term characterized by an artificial diffusion, so called numerical diffusion (Chung, 2002). Its value is directly linked to the mesh size: the smaller the mesh size, the lower the truncation error. This numerical diffusion adds to mass diffusion which leads to an overestimation of the mass fluxes. This effect is particularly significant at the droplets interface where the mass transport is purely diffusive and the concentration gradient important.

Table 1. Influence of the mesh grid size on simulations for a computational domain of 100 µm × 30 µm.

Node number	Δx (µm)	Δy (µm)	U_d (m/s)	U_c (m/s)	$(k_d a_{d,simu} V_{UC})/V_d$ (s^{-1})
125×30	0.80	0.30 to 1.66	0.1401	0.0877	122.6
250×30	0.40	0.30 to 1.66	0.1391	0.0872	121.2
125×75	0.80	0.40	0.1534	0.0945	95.7
160×75	0.625	0.40	0.1533	0.0945	94.0
125×100	0.80	0.30	0.1537	0.0949	91.4

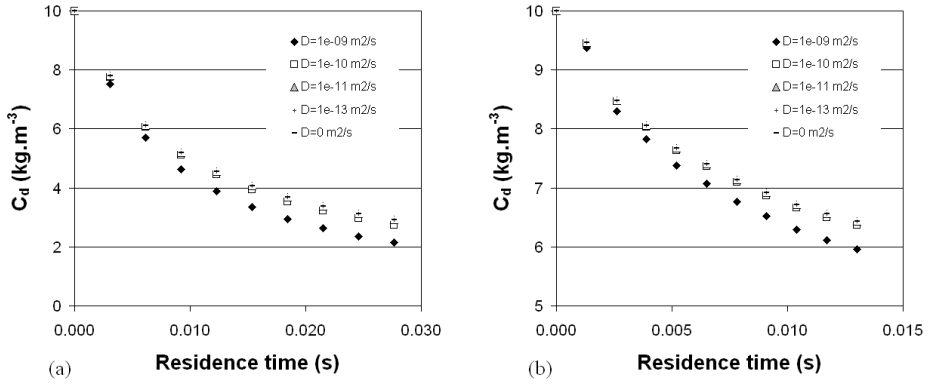

Fig. 3. Mean droplet concentration profile for various mass diffusion coefficients: (a) U_d = 0.0977 m/s, L_d = 53 µm, L_{UC} = 300 µm, Δx = 0.8 µm, Δy = 0.3 to 1.66 µm; (b) U_d = 0.2314 m/s, L_d = 150.4 µm, L_{UC} = 300 µm, Δx = 0.8 µm, Δy = 0.3 to 1.66 µm.

The numerical diffusion impact is highlighted on Figure 3. Indeed, it illustrates the mean droplet concentration profile $\overline{C}_d$ computed on a grid with 30 nodes (computational domain of 30 µm depth), with different mass diffusion coefficients D (D_d=D_c=D). We can see that even when this coefficient equals zero, the solute transfers from one phase to the other: this is purely an effect of the numerical diffusion. The profile is independent of the mass diffusion coefficient value when it is lower than 10^{-9} m^2/s. It means that the numerical diffusion for such a grid is in the order of magnitude of 10^{-9} m^2/s which is in the same range that common mass diffusion coefficients in liquids.

Figure 4 (a) reveals that when the computational domain of 30 µm depth is described by at least 75 nodes, the mean droplet concentration profile is independent of the mesh size for D=10^{-9} m^2/s (33% increase in the node number over the y-axis produces less than 5% variation in the computation results). It suggests that the numerical diffusion with such grids is negligible compared to common mass diffusion coefficients in liquids. Figure 4 (b) also shows that the concentration field computed on the 125×30 mesh grid with D equals to 10^{-9} m^2/s was equivalent to the one obtained on the finest grid (125×100) when D was set to 5.10^{-9} m^2/s. It means that the numerical diffusion on the 125×30 mesh grid can be estimated at 4.10^{-9} m^2/s. Therefore the sum of numerical and mass diffusions is still in the good order of magnitude to represent diffusion in liquid phases. Consequently, in spite of the numerical diffusion, we decided to employ thick grids (half a channel depth represented by at least 30 nodes) since it required reasonable computational times.

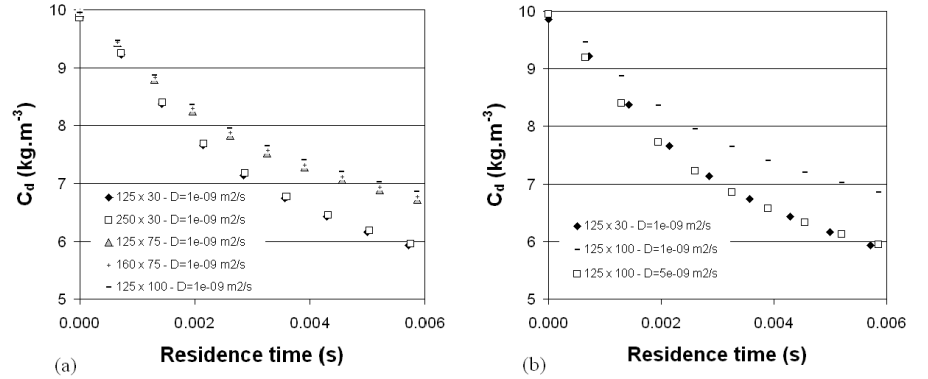

Fig. 4. Impact of the mesh grid size on the mean droplet concentration profile computation.

3. Results and discussions

As illustrated in Figure 5 (a), the hydrodynamic structures obtained in this study are analogous with those experimentally and numerically observed in previous works for slug flow in microchannels: internal vortices in both the continuous and dispersed phases and a thin film that wets the wall (Thulasidas et al., 1995; Kreutzer et al., 2005; Kashid et al., 2005; Taha and Cui, 2006).

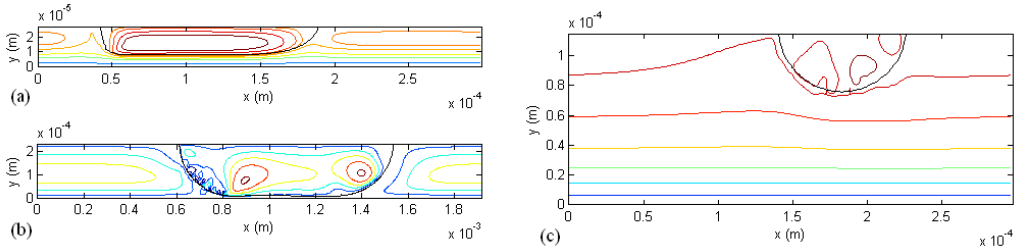

Fig. 5. Flow structures obtained by 2D computations with JADIM: (a) w_C = 60 µm, U_d = 0.1837 m/s, L_d = 147.2 µm, L_{UC} = 300 µm; (b) w_C = 480 µm, U_d = 0.0036 m/s, L_d = 924 µm, L_{UC} = 1920 µm; (c) w_C = 240 µm, U_d = 0.0144 m/s, L_d = 87 µm, L_{UC} = 300 µm.

We also obtained two other flow structures depending on the flow parameters as it is shown in Table 2 and Figure 6 (Sarrazin et al., 2007): (1) with several recirculation nodes in the droplets as shown in Figure 5 (b): this phenomenon was notably observed for low capillary and Reynolds numbers (low velocity and high interfacial tension), (2) without any recirculation loops in the continuous phase because the droplet is not enough confined (see Figure 5 (c)). This last structure can be related to Stokes flow (isolated droplet in an infinite medium at low Reynolds number) where the streamlines close to the droplets follow the interface shape. The impact of these structures on mass transfer will be afterwards discussed.

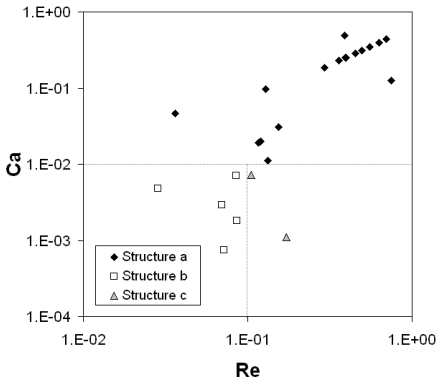

Fig. 6. Flow structures as a function of the Reynolds and the capillary number.

Table 2. Computations parameters

w_C (µm)	U_d (m/s)	L_{UC} (µm)	L_d (µm)	w_d (µm)	σ (N/m)	Flow Structure
50	0.0514	200	100.8	43.9	0.038	(a)
50	0.0616	300	154.4	43.9	0.038	(a)
60	0.0977	300	52.8	43.0	0.01	(a)
60	0.1199	300	54.4	43.0	0.01	(a)
60	0.1326	300	54.4	41.1	0.01	(a)
60	0.1653	300	56.0	41.1	0.01	(a)
60	0.1312	300	143.2	43.0	0.01	(a)
60	0.1312	900	143.2	43.0	0.01	(a)

60	0.1837	300	147.2	41.1	0.01	(a)
60	0.2314	300	150.4	41.1	0.01	(a)
60	0.1505	300	100.8	43.0	0.01	(a)
60	0.1505	600	100.8	43.0	0.01	(a)
60	0.1505	900	100.8	43.0	0.01	(a)
60	0.1505	1200	100.8	43.0	0.01	(a)
60	0.2500	195	151.2	41.1	0.01	(a)
60	0.2098	300	160.8	37.1	0.005	(a)
60	0.0121	300	126.4	49.4	0.005	(a)
60	0.1291	300	128.0	49.4	0.038	(a)
60	0.0398	240	119.2	53.3	0.038	(a)
60	0.0095	240	118.4	54.3	0.038	(b)
60	0.0386	300	121.6	53.3	0.038	(a)
120	0.0142	480	234.0	110.6	0.038	(b)
120	0.0221	300	84.8	78.6	0.038	(a)
240	0.0058	960	458.0	225.8	0.038	(b)
240	0.0144	300	87.0	79.9	0.038	(c)
480	0.0036	1920	924.0	457.2	0.038	(b)
960	0.0015	3840	1800.0	921.0	0.038	(b)
960	0.0022	300	86.0	82.2	0.038	(c)

3.1. Methodology for the identification of the mass transfer coefficient

The code developed for the computation of the solute transport from the dispersed phase to the continuous phase allows the calculation of the local solute concentration all along the microchannel. Figure 7 illustrates the computed concentration profiles as a function of the residence time in the three volumes representative of slug flows: (1) the droplet, (2) the interval, which is the volume between two successive droplets, (3) and the film. The division of the continuous phase into two distinct volumes is pertinent since the concentrations in the interval and the film are very different: the film saturates faster than the interval.
Moreover, it can be noticed that the concentration in the film can temporary overpass the steady state concentration. This phenomenon is particularly important for the case where the interval volume is high compared to the sum of the film and the droplet volumes (Figure 7 (a)). This is due to the time the interval requires to enrich in solute: if this interval is important compared to the droplet and the film, it takes a long time for this volume to be charged in solute compared to the saturation time of the film. Therefore, the homogenisation of the concentration in the film and the droplet occurs before the interval is totally charged. Then, the homogenisation over the all unit cell leads to a decrease of the film and the droplet concentrations to the final steady state concentration.

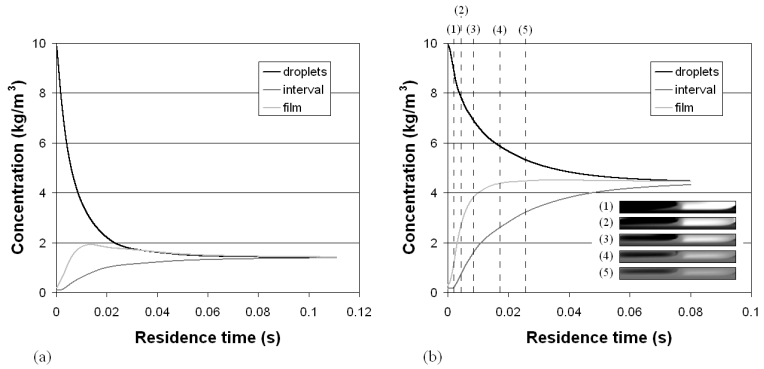

Fig. 7. Mean concentration profiles in the three volumes identified in a unit cell: (a) w_C = 60 µm; U_d = 0.1326 m/s, L_d = 54.4 µm, L_{UC} = 300 µm; (b) w_C = 60 µm; U_d = 0.1837 m/s, L_d = 147.2 µm, L_{UC} = 300 µm. The concentration field is depicted by means of a colour function (black for C = 0 kg.m^{-3}; white for C=C^0).

A local mass transfer coefficient $k_d a_{d,simu}$ is identified from the computed concentration field. It is obtained from a mass balance in a droplet, where the flux through the interface is modelled using this coefficient, the mean solute concentration in the droplets and the final concentration C_d^* obtained for an infinite time (Eq.35). V_d and V_{UC} respectively correspond to a droplet and a unit cell volume. The integrated formulation of Eq.35 directly leads to the mass transfer coefficient (Eq.36).

$$V_d \frac{\partial \overline{C_d}}{\partial t} = -k_d a_{d,simu} V_{UC} \left(\overline{C_d} - C_d^* \right) \tag{35}$$

$$\ln\left(\frac{\overline{C_d}^0 - C_d^*}{\overline{C_d} - C_d^*} \right) = \frac{k_d a_{d,simu} V_{UC}}{V_d} \cdot t \tag{36}$$

To obtain $k_{d,simu}$, the specific interfacial area a_d is calculated according to the capillary number Ca. In fact, Sarrazin et al. (2007) showed that the cross section shape of a droplet in square microchannels dependes on this number: for Ca higher than 0.04 the droplets body can be considered as cylindrical, while for Ca lower than 0.04 the dispersed phase tends to cling to the channel walls. This tendency was also suggested by Kreutzer et al. (2005) for gas-liquid slug flow. We consider the caps of the droplets have a spherical shape in both cases. Consequently, a_d is estimated using the following equations:

$$a_d = \frac{\pi \cdot w_d \cdot (L_d - w_d) + \pi \cdot w_d^2}{L_{UC} \cdot w_C^2} \qquad \text{for Ca} > 0.04 \tag{37}$$

$$a_d = \frac{4 \cdot w_d \cdot (L_d - w_d) + \pi \cdot w_d^2}{L_{UC} \cdot w_C^2} \qquad \text{for Ca} < 0.04 \tag{38}$$

3.2. Model for mass transfer coefficient

The influence of the flow parameters is determined through different simulation cases described in Table 2. The fluid properties are the same in all runs (ρ_c = 950 kg.m^{-3}, μ_c = 0.019 Pa.s; ρ_d = 1000 kg.m^{-3}, μ_d = 0.001 Pa.s; μ_d / μ_c = 0.053), except the interfacial tension σ which determines the droplets shape. In all the simulations, the initial concentration is set at 10 kg/m^3, the mass diffusion coefficient in both phases is equal to 10^{-9} m^2/s and the distribution coefficient m equal to 1. In order to study the relationship between the droplet side volumetric

mass transfer coefficient and the flow parameters, we assumed that this coefficient could be modelled in terms of Eq.39, where d_d is the droplet volume equivalent diameter defined by Eq.40 and ε the ratio between the volume of a droplet and a unit cell ($\varepsilon = V_d / V_{UC}$).

$$k_d = \alpha \cdot U_d^{p1} \cdot w_C^{p2} \cdot d_d^{p3} \cdot \varepsilon^{p4} \cdot \sigma^{p5} \tag{39}$$

$$d_d = 2 \cdot \sqrt[3]{\frac{3}{4\pi} V_d} \tag{40}$$

The parameters α and p_i are identified to fit the simulation results. It lead to Eq.41, where the term $k_d d_d$ can be related to a Sherwood number, $U_d w_C$ to a Reynolds number and (U_d / σ) to a capillary number. The term (w_C / d_d) shows the positive impact of the confinement on mass transfer. The power 0.69 that illustrates the dependency of Reynolds number on mass transfer is in the good order of magnitude. Indeed, we can relate it to the common dependency of discontinuous phase mass transfer coefficient in particle Reynolds number, where the power equals 0.371 (Eq.1). The proposed correlation shows that the mass transfer coefficient decreases when the capillary number increases. This tendency can be explained by the influence of this number on the flow structure in the droplets. In fact, for low values of the capillary numbers, Sarrazin et al. (2007) show that very small recirculation loops appear at the front of the droplets. This effect tends to increase the mixing efficiency in the dispersed phase, to the benefit of the mass transfer (reduction of the resistance to the transfer in the droplets). Nevertheless, regarding the dependency of the term (U_d / σ) on mass transfer, this effect has a minor influence compared to the Reynolds number and the confinement impact. The parameter α is equal to 2.77e-04 (Figure 8). However, this value is obtained by fitting 2D results, and would have probably been different if we had carried out 3D simulations. Moreover, this parameter value depends on the fluid properties.

$$k_d d_d = \alpha \cdot \varepsilon^{0.17} \cdot (U_d w_C)^{0.69} \cdot \left(\frac{U_d}{\sigma}\right)^{-0.07} \cdot \left(\frac{w_C}{d_d}\right)^{0.75} \tag{41}$$

Figure 8 shows that this correlation allows a good fitting of the simulation results as far as the hydrodynamic behaviour of the droplets correspond to flow structure (a). Indeed, the correlation underestimates mass transfer for structure (b), and it overestimates it for structure (c). This can be explained by: (1) the recirculation nodes in flow structure (b) that increase the transfer by enhancing the mixing in the dispersed phase and (2) the lack of recirculation loops in the continuous phase in flow structure (c) that slows down the solute transport in that phase compared to the transport phenomenon in flow structure (a). However the global trends of the curves obtained for all flow structures are roughly the same. This means that mass transfer evolves with the flow parameters in the same way whatever is the flow structure. The main difference in the mass transfer coefficient estimation will be the value of the parameter α.

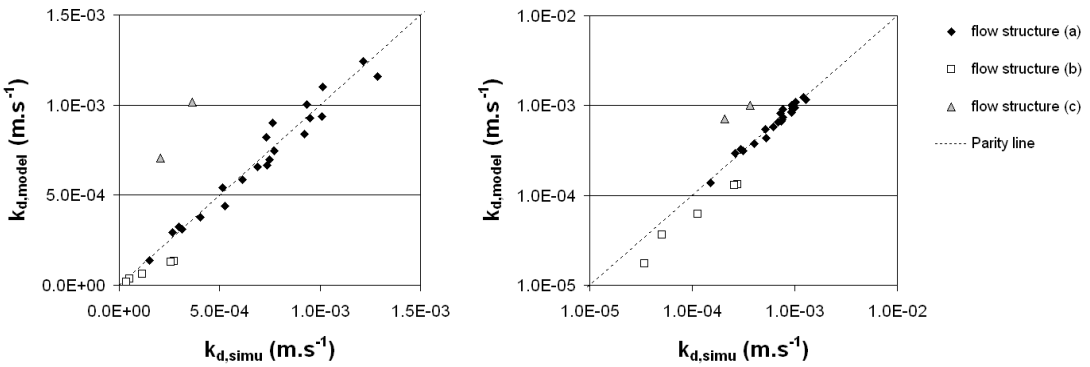

Fig. 8. Simulation results fitting with Eq.41.

Finally, we compared the simulation results with the coefficients obtained from the models and correlations described in part 1 as illustrated in Figure 9. Regarding the correlation suggested by Skelland and Wellek, the difficulty is to use the pertinent characteristic parameters to calculate the dimensionless numbers. In order to have a correlation easy to be applied, we focused on parameters that can simply be estimated. Therefore, mass transfer coefficient with this correlation has been estimated using the following formulation of Eq.1:

$$Sh_d = \frac{k_d d_d}{D_d} = 31.4\left(\frac{\rho_c U_d d_d}{\mu_c}\right)^{0.371}\left(\frac{\mu_c U_d}{\sigma}\right)^{0.371}\left(\frac{4D_d\cdot(L_d - w_d + \pi w_d/2)}{{d_d}^2\cdot U_d}\right)^{-0.338}\left(\frac{\mu_d}{\rho_d D_d}\right)^{-0.125} \quad (42)$$

where the particle Fourier number Fo_d depends on a contact time defined as the ratio between a contact length and the droplets velocity U_d. The contact length has been estimated as the length of the interface travelled by a fluid element of the droplets as shown in Eq.43 (i.e. a fluid element of the vortex external streamline). The characteristic length used is half a droplet diameter which represents the characteristic length of diffusion inside the droplets.

$$Fo_d = \frac{D_d}{t_e (d_d/2)^2} \quad (43)$$

$$t_e = \frac{(L_d - w_d) + \pi w_d/2}{U_d} \quad (44)$$

As illustrated in Figure 9, this formulation leads to two different trends for low and high values of mass transfer coefficients. In fact, this correlation is used to model mass transfer within circulating droplets: it does not consider the difference in flow structure. Moreover, it was proposed for macrochannels where the droplets are not constrained by the channel wall while we noticed an enhancement of mass transfer with the confinement factor. The model of van Baten and Krishna suggested for gas-liquid slug flow leads to a good global trend. However, it allows the calculation of continuous phase side mass transfer coefficients. Therefore, it could possibly be used when the resistance to transfer in the droplets is negligible compared to the resistance in the continuous phase (flow structure (b) with high recirculation motion). Finally the correlation proposed by Bercic and Pintar leads to a high scattering when trying to fit the simulation results. Nevertheless, their correlation, which was suggested from experiments in channels of more than 1 mm diameter, is independent of the channel size while Vandu et al. (2005) shows the importance of this parameter on mass transfer.

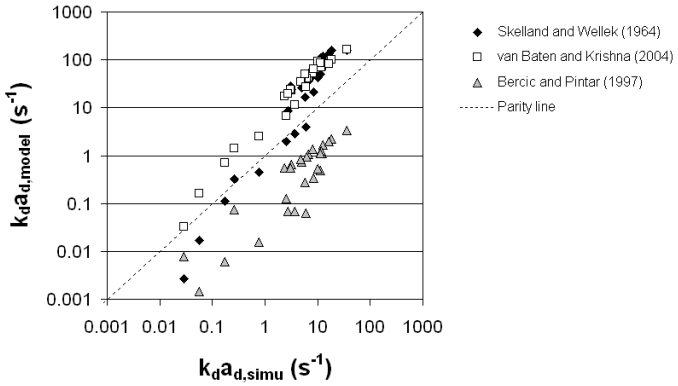

Fig. 9. Comparison of the mass transfer coefficients obtained by simulation and with literature models.

4. Conclusions

In this study, liquid-liquid mass transfer in square microchannels was investigated using 2D simulations. The hydrodynamic and the concentration field computations were decoupled and Marangoni effects were not taken into account. However, it allowed the study of general tendencies, i.e. how mass transfer is influenced by the flow conditions and the channel size. This work showed that the confinement factor in microchannels allows an enhancement of mass transfer compared to what can be obtained in macrochannels. Moreover, this study reveals that the flow structures had a major impact on the mass transfer coefficient estimation. Indeed, while the general trend is the same for all flow structures (i.e. same dependencies of the mass transfer coefficients in the flow parameters), mass transfer is enhanced by the mixing efficiency in the droplets. This is logically linked to the number of recirculation nodes in the dispersed phase. However, flow structures with several recirculation nodes are obtained for low droplets velocities which do not favour mass transfer.
In order to complete this work, the influence of the fluid properties has to be studied. We could also simulate mass transfer coupling hydrodynamics and mass transfer, i.e. taking into account the impact of the solute transfer on the hydrodynamics. This should notably allow a better prediction of this process with concentrated phase. Finally, an experimental study will be implemented in order to validate the correlation obtained.

Acknowledgments

This work has been supported by 6th Framework EU under Grant IMPULSE No: NMP2-CT-2005-011816 and the Institut National Polytechnique of Toulouse (see http://www.inp-toulouse.fr). Experiments presented in this paper were carried out using the Grid'5000 experimental testbed, an initiative from the French Ministry of Research through the ACI GRID incentive action, INRIA, CNRS and RENATER and other contributing partners (see https://www.grid5000.fr).

Notation

a specific interfacial area, $m^2.m^{-3}$
Ca capillary number, dimensionless
C local concentration in solute, $kg.m^{-3}$
$\hat{C}$ transformed concentration in solute, $kg.m^{-3}$

$\overline{C}$	mean concentration in solute, $kg.m^{-3}$
d	diameter, m
D	mass diffusion coefficient, $m^2.s^{-1}$
Fo	Fourier number, dimensionless
k	mass transfer coefficient, $m.s^{-1}$
L	length, m
m	distribution coefficient
n	unit vector normal to the interface
p_i	fitting parameters defined by Eq.39
P	pressure, Pa
Re	Reynolds number, dimensionless
S	Strain tensor, $m.s^{-2}$
Sc	Schmidt number, dimensionless
Sh	Sherwood number, dimensionless
t	time or residence time, s
$\hat{t}$	transformed time, s
t_e	contact time, s
T	flow period, s
T	viscous stress tensor, $N.m^{-2}$
u	velocity vector, $m.s^{-1}$
$\hat{\mathbf{u}}$	transformed velocity vector, $m.s^{-1}$
U	velocity, $m.s^{-1}$
V	volume, m^3
x	coordinate over the length, m
w	width, m
y	coordinate over the width, m

Subscripts and Superscripts

C	channel
c	continuous phase
cap	refers to the droplets caps
d	dispersed phase (droplet or bubble)
film	refers to the film that wets the channel walls
k	computation cell index
L	liquid phase
model	refers to data calculated with a model
simu	refers to data obtained by simulations
UC	unit cell

Superscripts

^{0}	refers to the initial time
*	refers to the equilibrium state
‘	refers to the frame of reference moving with the droplets

Greek letters

α	fit parameter
δ	thickness, m

δ_I Dirac-delta-function
Δ parameter defined by Eq.8
Δx computational cell length, m
Δy computational cell width, m
ε ratio between a droplet and a unit cell volume
ε_G gas hold-up
μ_l linear viscosity, Pa.s
μ_h harmonic viscosity, Pa.s
ρ density, $kg.m^{-3}$
σ interfacial tension, N.m
φ local volume fraction

References

Benkenida, A., Magnaudet, J. (2000). Une méthode de simulation d'écoulements diphasiques sans reconstruction d'interfaces. C. R. Acad. Sci. Série IIb 328 (1), 25-32.

Berčič, G., Pintar, A. (1997). The role of gas bubbles and liquid slug lengths on mass transport in the Taylor flow through capillaries. Chem. Eng. Sci. 52 (21-22), 3709-3719.

Bonometti, T. (2005). Développement d'une méthode de simulation d'écoulements à bulles et à gouttes. Ph.D. Thesis, Institut National Polytechnique de Toulouse, Toulouse (France).

Brackbill, J.U., Kothe D.B., Zemach, C. (1992). A continuum method for modeling surface tension. J Comput Phys 100, 335-354.

Burns, J.R., Ramshaw, C. (2001). The intensification of rapid reactions in multiphase systems using slug flow in capillaries. Lab Chip 1, 10-15.

Chung, T.J. (2002). Computational fluid dynamics. Cambridge University Press.

Dummann, G., Quittmann, U., Gröschel, L., Agar, D.W., Wörz, O., Morgenschweis, K. (2003). The capillary-microreactor: a new reactor concept for the intensification of heat and mass transfer in liquid-liquid reactions. Catalysis Today 79-80, 433-439.

Hessel, V., Angeli P., Gavriilidis, A., Löwe, H. (2005). Gas-liquid and gas-liquid-solid microstructured reactors: contacting principles and applications. Ind. Eng. Chem. Res. 44, 9750-9769.

Irandoust, S., Ertlé, S., Andersson, B. (1992). Gas-liquid mass transfer in Taylor flow through a capillary. Canadian Journal of Chemical Engineering, 70, 115-119.

Jähnisch, K., Hessel, V., Löwe, H., Baerns, M. (2004). Chemistry in microstructured reactors. Angew. Chem. Int. Ed. 43, 406-446.

Kashid, M.N., Gerlach, I., Goetz, S., Franzke, J., Acker, J.F., Platte, F., Agar, D.W., Turek, S. (2005). Internal circulation within the liquid slugs of a liquid-liquid slug-flow capillary microreactor. Ind. Eng. Chem. Res. 44, 5003-5010.

Knudsen, J.G, Hottel H.C., Sarofim, A.F., Wankat P.C., Knaebel, K.S. (1998). Heat and mass transfer, in: Perry, R.H., Green, D.W., Perry's chemical engineer's handbook, 7th edition, McGraw-Hill, Section 5.

Kreutzer, M.T. (2003). Hydrodynamics of Taylor flow in capillaries and monolith reactors. Ph.D. thesis, Delft University of Technology, Delft (the Netherlands).

Kreutzer, M.T., Kapteijn, F., Moulijn, J.A., Heiszwolf, J.J. (2005). Multiphase monolith reactors: chemical reaction engineering of segmented flow in microchannels. Chem. Eng. Sci. 60, 5895-5916.

Legendre, D., Magnaudet, J. (1998). The lift force on a spherical bubble in a viscous linear shear flow. J. Fluid Mech. 368, 81-126.

Sarrazin, F., Loubière, K., Prat, L., Gourdon, C., Bonometti, T., Magnaudet, J. (2006). Experimental and numerical study of droplets hydrodynamics in microchannels. AIChE Journal 52 (12), 4061-4070.
Sarrazin, F., Bonometti, T., Prat, L., Gourdon, C., Magnaudet, J. (2007). Hydrodynamic structures of droplets engineered in rectangular micro-channels. Microfluid Nanofluid, article in press.
Slater, M.J. (1994). Rate coefficients in liquid-liquid extraction systems, in: Godfrey, J.C., Slater, M.J., Liquid-liquid extraction equipment, John Wiley & sons, pp. 45-94.
Skelland, A.H.P, Wellek, R.M. (1964). Resistance to mass transfer inside droplets. AIChE Journal 10 (4), 491-496.
Stankiewicz, A.I., Moulijn, J.A. (2000). Process intensification: transforming chemical engineering. Chem. Eng. Prog. 96 (1), 22-34.
Taha, T., Cui, Z.F. (2006). CFD modelling of slug flow inside square capillaries. Chem. Eng. Sci. 61, 665-675.
Thulasidas, T.C., Abraham, M.A., Cerro, R.L. (1995). Bubble-train flow in capillaries of circular and square cross section. Chem. Eng. Sci. 50 (2), 183-199.
van Baten, J.M., Krishna, R. (2004). CFD simulations of mass transfer from Taylor bubbles rising in circular capillaries. Chem. Eng. Sci. 59, 2535-2545.
Vandu, C.O., Liu, H., Krishna, R. (2005). Mass transfer from Taylor bubbles rising in single capillaries. Chem. Eng. Sci. 60, 6430-6437.
Yang, C., Mao, Z.-S. (2005). Numerical simulation of interphase mass transfer with the level set approach. Chem. Eng. Sci. 60, 2643-2660.
Yue, J., Chen, G., Yuan, Q., Luo, L., Gonthier, Y. (2007). Hydrodynamics and mass transfer characteristics in gas-liquid flow through a rectangular microchannel. Chem. Eng. Sci. 62, 2096-2108.